Stochastic Variation of the Aero-Thermal Flow Field in a Cooled High-Pressure Transonic Vane Configuration

STOCHASTIC VARIATION OF THE AERO-THERMAL FLOW FIELD IN A COOLED HIGH-PRESSURE TRANSONIC VANE CONFIGURATION

S. Salvadori[1] - M. Carnevale[2] - R. Ahlfeld[3] - F. Montomoli[3] – F. Martelli[1]

[1]DIEF, University of Florence, via di S. Marta, 3 – 50139 Firenze, Italy
[2]VUTC, Department of Mechanical Engineering, Imperial College London, SW7 2BX, UK
[3]UQ LAB, Department of Aeronautical Engineering, Imperial College London, SW7 2BX, UK

ABSTRACT

In transonic high-pressure turbine stages, oblique shocks originated from vane trailing edges impact the rear suction side of each adjacent vane. High-pressure vanes are usually cooled to tolerate the combustor exit temperature levels, which would reduce dramatically the residual life of a solid vane. Then, it is highly probable that shock impingement will occur in proximity of one of the coolant rows. It has already been observed that the presence of an adverse pressure gradient generates non-negligible effects on heat load due to the increase in boundary layer thickness and turbulence level, with a detrimental impact on the local adiabatic effectiveness values. Furthermore, the generation of a tornado-like vortex has been recently observed that could further decrease the efficacy of the cooling system by moving cold flow far from the vane wall. It must be also underlined that manufacturing deviations and in-service degradation are responsible for the stochastic variation of geometrical parameters. This latter phenomenon greatly alters the unsteady location of the shock impingement and the time-dependent thermal load on the vane. Present work starts from what is shown in literature and provides a highly-detailed description of the aero-thermal field that occurs on a model that represents the flow conditions occurring on the rear suction side of a cooled vane. The numerical model is initially validated against the experimental data obtained by the University of Karlsruhe during TATEF2 EU project, and then an uncertainty quantification methodology based on the probabilistic collocation method and on Padè's polynomials is used to consider the probability distribution of the geometrical parameters. The choice of aleatory unknowns allows to consider the mutual effects between shock-waves, trailing edge thickness and hole diameter. Turbulence is modelled by using the Reynolds Stress Model already implemented in ANSYS® Fluent®. Special attention is paid to the description of the flow field in the shock/boundary layer interaction region, where the presence of a secondary effects will completely change the local adiabatic effectiveness values.

KEYWORDS: Uncertainty Quantification, Film Cooling, Shock Waves, CFD, RSM

NOMENCLATURE

A	[m^2]	area
D	[m]	diameter
Ma	[-]	Mach number
Pr	[-]	Prandtl number
T	[K]	temperature
X	[m]	stream-wise coordinate
Y	[m]	pitch-wise coordinate
Z	[m]	span-wise coordinate

Subscripts & Superscripts

0	total or stagnation
aw	adiabatic wall
c	coolant
f_ω	Probability Density Function
is	isentropic
m	hot gas
nd	non-dimensional
nom	nominal
P_n	Legendre polynomial of n^{th} order
rec	recovery
te	trailing edge
$\hat{u}_n$	Polynomial Chaos expansion coefficients
$u(x,\omega)$	a solution depending on physical variable x and random variable ω
w	wall

Greek

γ	[-]	isentropic exponent
η	[-]	effectiveness
ω_j		Gauss-Lobatto integration weights

Acronyms

BR	[-]	Blowing Ratio
CFD		Computational Fluid Dynamics
EXP		Experimental
RANS		Reynolds-Averaged Navier-Stokes
RSM		Reynolds Stress Model
TE		Trailing Edge
UQ		Uncertainty Quantification

INTRODUCTION

A widely-used strategy to increase efficiency and specific power output of gas turbines consists in increasing the turbine entry temperature. Therefore, metal temperatures approach the melting point of the alloys used in high-pressure nozzles and the stators are more and more loaded as shown by Salvadori *et al.* (2001). Advanced cooling systems such as film cooling are necessary to protect nozzles from high temperature. The interaction of the coolant with the main-flow increases complexity in the flow's structures. Andreopulos and Rodi (1984) have identified a pair of counter-rotating vortices with a velocity component perpendicular to the surface. This structure has been named "kidney-shaped vortices". These vortices are generated by the redistribution of the vorticity content in the boundary layers, and play a key role in the performances of the cooling devices. A lift-off effect is generated, which transport the coolant away from the wall with a detrimental effect on the surface coverage. Leboeuf and Sgarzi (2001) numerically investigated these three-dimensional structures over flat plates. They noticed that the kidney vortices are greatly influenced by the flow behaviour inside of the orifice. An additional vortical structure, the so called "tornado effect", has been originally individuated by Hagen and Kurosaka (1993). They demonstrated the presence of a core-wise, cross-flow transport in hairpin vortices (created by coolant injection) in the laminar boundary layer. This core-wise phenomenon continuously moves the fluid from the wall to the free stream. Similar structures were observed for a turbulent boundary layer in a previous research by Chen and Blackwelder (1978) and in presence of shocks by Carnevale *et al.* (2014).

The effect of hole's shape and location have also been studied. Montis *et al.* (2014) investigated the effect of the cooling position on the losses of a turbine stage. In high-pressure stages, oblique shocks shed from the Trailing Edge (TE) impinge onto the suction side of the adjacent vane. In case

of presence of a row of film cooling holes their effectiveness is affected by the three-dimensional interaction between the cooling flow, the boundary layer development and the shock itself. Ligrani *et al.* (2001), Ochs *et al.* (2007) and Salvadori *et al.* (2013) demonstrated a non-negligible variation in the local value of adiabatic effectiveness when the hole is located a few diameters before the shock impingement zone. Furthermore, Montomoli *et al.* (2012) demonstrated that small variations in the coolant duct geometry affect the coolant flow redistribution in a non-negligible way. They employed Uncertainty Quantification (UQ) methodologies to highlight the importance of stochastic studies to obtain a reliable comparison with experimental data.

In this work the effect of the impinging shock is reproduced in a test case designed by the Institut fur Thermische Stroemungsmaschinen in Karlsruhe (see Ochs *et al.*, 2007 for details). A shaped plate positioned at the mid-height of a converging nozzle creates a diverging region where the Mach number reaches $Ma = 1.5$, while at the end of the plate the flow slows down through a shock system. Two geometrical parameters have been perturbed to introduce the uncertainty due to manufacturing deviations, namely the diameter of both the plate TE and the cooling hole. The stochastic distribution of adiabatic effectiveness is obtained using a probabilistic collocation method with Padè's polynomials. Laymaa and Heidmann (2003) already faced the sensitivity to uncertainty of film cooling devices but herein an innovative approach has been used to deal with the un-dumped oscillations associated to the Runge's phenomenon for higher order polynomial. Present work shows that the impact of uncertainty is relevant where the shock interacts with the coolant and the boundary layer.

TEST CASE DESCRIPTION

A numerical simulation of the proposed configuration has been previously performed by Salvadori *et al.* (2013) using a deterministic approach. Figure 1a shows a sketch of the test case, which includes the converging nozzle, the central (shaped) plate, the cylindrical cooling hole and the plenum. The main-flow reaches sonic speed at the throat while the shape of the lower part of the contoured plate allows the flow to accelerate further to supersonic velocities. At the trailing edge an oblique shock wave is generated, impinging on the lower wall in a region immediately after the cooling hole exit position. The flow physics is depicted in Figure 1b, which has been obtained for the nominal conditions during the current numerical campaign. The coolant interacts with the main-flow generating a weak shock, which merges with the oblique shock shed by the plate trailing edge that impinges on the lower wall. It is expected that the adiabatic effectiveness will be modified by the adverse pressure gradient that is responsible for a local growth of the boundary layer.

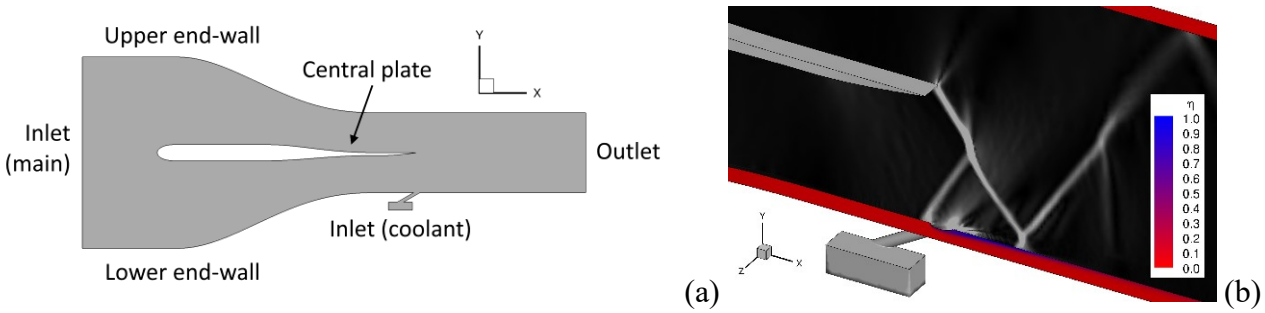

Figure 1: Control volume (a) and flow features (b)

In the experimental apparatus, five injection holes are located upstream of the shock impingement position and have a pitch-to-diameter ratio of 4 (see Ochs *et al.*, 2007). The control volume selected for the numerical campaign includes only a portion of the entire domain, being the channel symmetric along the hole mid-plane and between two adjacent holes. Therefore, the computational domain is limited in the z direction by two planes of symmetry, which are set normal to the x-z plane (use Figure 1b for reference). This choice neglects the formation of coolant

oscillations on planes parallel to the *x-z* plane, and is coherent with the steady nature of the computations presented in the present work. The theoretical free stream Mach number at the shock location is around $\mathrm{Ma} = 1.5$ and the blowing ratio $\mathrm{BR} = 1.0$ has been selected. The non-dimensional coolant total pressure is 1.01 with respect to main-flow inlet total pressure and the non-dimensional coolant total temperature is 0.557 with respect to main-flow inlet total temperature. For each investigated case, the numerical BR value has been calculated using the formula in Eq. 1, in accordance with the experimental definition:

$$BR = \frac{\dot{m}_c}{\dot{m}_m} \cdot \frac{A_m}{A_c} \tag{1}$$

It must be pointed out that the aim of the present work is not to reproduce exactly the experimental data but only to capture the flow features, and then to quantify the uncertainty associated with the hole diameter and the plate trailing edge dimensions. The impact of geometrical uncertainties on the adiabatic effectiveness is evaluated using the following definition:

$$\eta_{aw} = \frac{T_{aw} - T_{rec,m}}{T_{0,c} - T_{rec,m}} \tag{2}$$

Calculations with an adiabatic condition for the cooled plate are used to evaluate the adiabatic wall temperature distribution T_{aw}. The evaluation of the main-flow recovery temperature $T_{rec,m}$ has been performed using Eq. 3:

$$T_{rec,m} = T_{0,m} \cdot \frac{1 + \mathrm{Pr}^{0.33} \frac{\gamma - 1}{2} Ma_{is}^2}{1 + \frac{\gamma - 1}{2} Ma_{is}^2} \tag{3}$$

The aim of the present work is to analyse the accuracy of CFD simulations in the evaluation of the cooling efficacy in such kind of configuration and the impact of stochastic uncertainties in the evaluation of the centreline adiabatic effectiveness.

GRID AND TEST-CASE MODELING

The computational domain assumes flow symmetry at the hole centreline and between two adjacent holes. Therefore, the control volume includes the main-flow inlet, a coolant supply plenum and the cylindrical cooling channel, the end-walls that define the nozzle, the central shaped plate and the outlet. The importance of the plenum in film cooling simulations has been demonstrated by Garg and Rigby (1998) and more recently by Acharya and Leedom (2012) using large eddy simulations. That is the reason why the plenum has been included in the control volume. In the present calculations, steady Reynolds-Averaged Navier-Stokes (RANS) equations are solved. In this work a pressure-based approach has been selected. Pressure and density equations are coupled and the calculation is fully second order accurate. The Reynolds Stress Model (RSM) already implemented in the ANSYS® FLUENT® code (Launder *et al.*, 1975) has been used as turbulence closure to consider the anisotropic behaviour of turbulence, whose impact on the shock/coolant interaction could be crucial to match the real distribution of adiabatic effectiveness. Inlet turbulence level is set at 5% while a turbulence length scale of 1*mm* has been considered. Walls have been set as adiabatic and viscous heating has also been considered to make the heat transfer evaluation accurate. Calculation is converged when all the residuals are constantly below 10^{-4} and the mass-flow error is below 1%.

The meshes used for the nine calculations (necessary for the UQ analysis) has been generated using the commercial hybrid grid generator Centaur^{TM} by Centaursoft. The mesh is denser in the region where the shock-boundary layer interaction is expected (see Figure 2a) and the overall quality of the mesh is high. The number of tetrahedral elements in the coolant hole has been increased as shown in Figure 2b, with a very high resolution of the channel flow. The generated grids are particularly accurate in the near-wall region, where a value of y^+ always below 0.3 has been obtained for the first layer. The final mesh shown in Figure 2a and Figure 2b is the one used for the nominal case and contains approximately 8M elements. All the generated meshes include a similar number of elements and are generated using the same elements distribution.

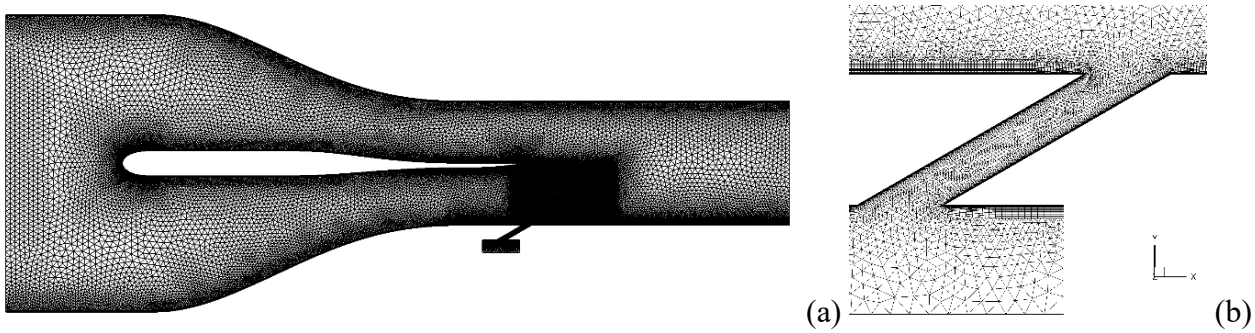

(a) (b)

Figure 2: Computational grid: whole domain (a) and detail of the hole region (b)

SHOCK-BOUNDARY LAYER INTERACTION WITH COOLANT

Figure 3a shows the comparison between the numerical and experimental maps of adiabatic effectiveness as defined in Eq. 2. As can be observed, the lateral spreading of the cooling flow is underestimated by CFD with respect to the experiments. The coolant flow seems to be confined in the centreline by the numerical simulation, where the experiments show a wider (and non-symmetric) redistribution of the flow coming from the cylindrical hole. It could be observed that results obtained using RSM are closer to the experiments with respect to the data shown by Salvadori *et al.* (2013), obtained using the *k-ω* model by Wilcox (2004). This result can be explained considering the anisotropy of the RSM, which allows for a more pronounced lateral pitch-wise mixing of the coolant with the hot gas.

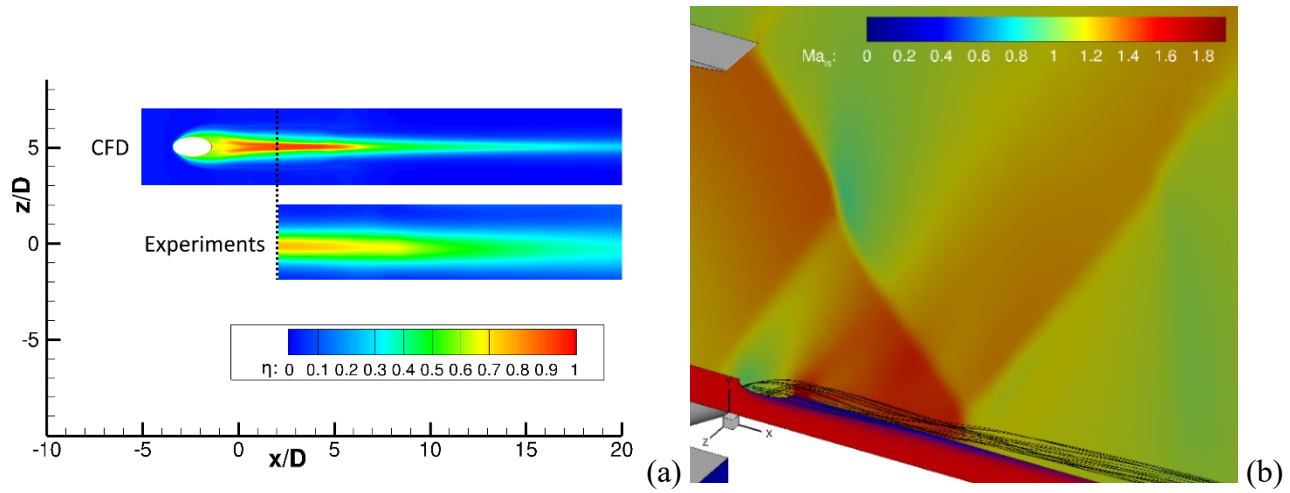

(a) (b)

Figure 3: Comparison of adiabatic effectiveness maps obtained by CFD and experiments (a) and streamlines behaviour in the shock impingement region (b) for the nominal case

Present results can also be discussed considering Figure 5, where the experimentally evaluated centreline adiabatic effectiveness is compared with the numerical data, including the data obtained for "Grid 5", which is the baseline (deterministic) configuration. As can be observed, up to *x/D* =

7.0 numerical data overestimate the adiabatic effectiveness (+30% at x/D = 4.0), while after that location there is an underestimation up to -25% at x/D = 15.0. This behaviour could be associated to a wrong prediction of the shock impingement location and interaction with coolant. Numerical simulation suggests that shock impinges on the lower end-wall at approximately x/D = 5.0, where the slope of the curve changes by a non-negligible factor, while experimental data suggest x/D = 8.0. This wrong prediction could be ascribed to the inherently unsteady nature of the phenomena under evaluation. In fact, the oblique shock is expected to oscillate on the x-y plane due to the vortex shedding which occurs at the trailing edge of the plate. It is well known from fluid dynamics that the correct intensity of a shock can be correctly captured only by an unsteady analysis due to non-linear, unsteady stress terms (He, 2003). Therefore, the pressure field in the hole exit region is time-dependent and the coolant redistribution could shed on the x-z plane thus leading to an enhanced lateral spreading. Since no information about the shock oscillation is available from the experiments, it is not possible to analyse this topic unless unsteady CFD is performed, which is not the aim of the present work. As a first conclusion, we can say that steady numerical simulations cannot capture exactly the adiabatic effectiveness values due to missing non-linear interaction features, and then only the overall behaviour of the coolant/shock interaction will be described here.

A detailed analysis has been performed to better understand why the centreline adiabatic effectiveness reduces its value after the shock location. This can be explained looking at the streamlines exiting from the coolant flow for the nominal case. In Figure 3b, the isentropic Mach number distribution on the cooling hole symmetry plane, the adiabatic effectiveness lines on the lower end-wall and the streamlines exiting from the cooling hole are shown. As can be observed, the cold flow is initially kept near the lower wall, coherently with the adiabatic effectiveness maps and with a numerical BR = 0.83, which is slightly lower than the experimental value and suggests a lower jet penetration in the main-flow. A few diameters later (approximately x/D = 5.0) the adverse pressure gradient associated with the shock impingement generates a lift-off effect of the coolant. In that region, the boundary layer height is increased by the shock impingement and the cooling flow is furtherly detached from the wall. After the shock interaction, the coolant flow does not reattach, which explains why the adiabatic effectiveness values shown in Figure 5 decrease so sharply. This behaviour is coherent with the presence of the already mentioned tornado-like vortex, which per Carnevale *et al.* (2014) enhances the local reduction of cooling effectiveness in presence of shocks.

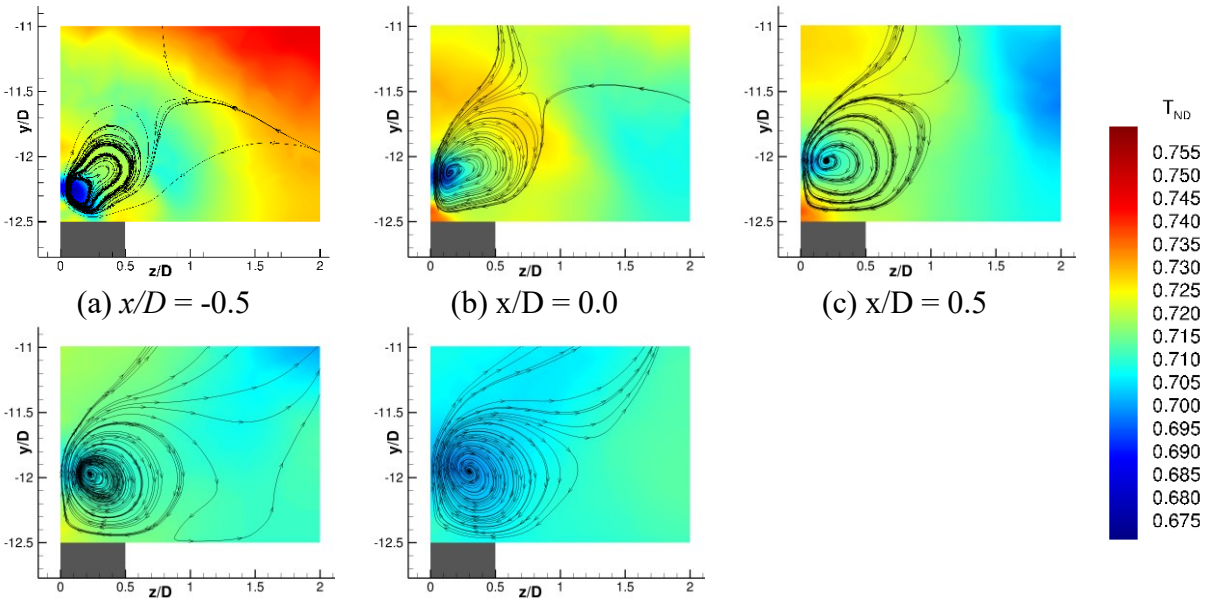

(a) x/D = -0.5 (b) x/D = 0.0 (c) x/D = 0.5

(d) x/D = 1.0 (e) x/D = 1.5

Figure 4: Non-dimensional temperature maps and streamlines in the hole/shock region

A detailed analysis of the local interaction between the main-flow and the cooling flow is reported in Figure 4, where a series of slices perpendicular to the end-wall are reported considering a region between the hole and the shock impingement position. For reference purposes, it is useful to know that the hole trailing edge is positioned at *x/D* = -1.5 and that the images in Figure 4 include the region between *x/D* = -0.5 and *x/D* = 1.5. Streamlines are superimposed on the non-dimensional temperature profiles (with respect to the main-flow inlet total temperature) to visualize the local vortex formation and the cooling flow redistribution. As can be observed, the cooling flow is initially positioned next to the end-wall (*x/D* = -0.5, Figure 4a) and a strong recirculation vortex (that comes from inside of the hole itself) is present. That vortex is responsible for the rapid movement of the coolant flow far from the wall. Then, the vortical structure moves far from the wall while main-flow is mixed with coolant until the latter is detached from the end-wall until a complete mixing is obtained at *x/D* = 1.5 (Figure 4e). Flow structures are close to what is usually shown in literature and do not seem to be affected by the presence of the shock impingement.

STATISTICAL APPROACH

A non-intrusive statistical approach has been used to assess the effect of geometry deviation on film cooling performance in presence of shocks. It is based on a polynomial description of the stochastic variation. Polynomial Chaos (PC) expansions are a computationally very efficient approach to quantify model variation for a small number of input uncertainties. An extensive review for such methods is available in Montomoli *et al.* (2015). Carnevale *et al.* (2013) applied a subclass of these methods (Probabilistic Collocation Methods, PCM) based on Hermite's polynomials, for heat transfer predictions for internal cooling devices. However, PCM techniques, such as all purely continuous polynomial expansions, are not suitable when a discontinuity is present in the system response.

In shock dominated problems (such as the present case study) the most suitable is the Padè approximation as introduced by Chantrasmi *et al.* (2009). The Padè approximation is a generalisation of Polynomial Chaos where a discontinuous response surface is described by a ratio of PC expansions. As this expansion can have poles, it can describe discontinuities. Numerator and denominator of the rational function are determined through finite sums of orthogonal basis polynomials whose coefficients can be calculated from the function values at a predefined set of points. Examples of this include Padè-Jacobi, Padè-Chebischev and Padè-Legendre approximants. Padè-Legendre (PL) approximants are used in the present work as described by Hesthaven *et al.* (2006) and Chantrasmi *et al.* (2009).

A complete basis of Legendre polynomials is defined by:

$$\langle P_n, P_m \rangle = \frac{1}{n + 1/2} \delta_{n,m} \quad with \quad n, m \in \mathbb{N} \cup \{0\} \tag{4}$$

Polynomials are defined uniquely as $(1, x, {}^{1}/_{2}\,(3x^2 - 1), \dots)$ and the expansion can be continued to any desired order. Every function u can be defined as a linear combination of Legendre's basis:

$$u = \sum_{n=0}^{\infty} \hat{u}_n P_n \tag{5}$$

The coefficients $\hat{u}_n$ in the n^{th} Legendre coefficient of u are defined as follows:

$$\hat{u}_n = \langle u, P_n \rangle / \langle P_n, P_n \rangle \tag{6}$$

The function is known in specific discrete points and the Gaussian quadrature provides the discrete formulation where each scalar product in Eq. 6 is defined as follow:

$$\langle P_n, P_m \rangle_N = \sum_{j=0}^{N} P_n(x_j) P_m(x_j)\, \omega_j \quad with \quad \omega_j = \frac{2}{N(N+1)\left[P_N(x_j)\right]^2} \tag{7}$$

The nodes x_j in Eq. 7 are the quadrature points and ω_j are the quadrature weights of the Gauss-Lobatto quadrature rule as described by Abramowitz and Stegun (1965). The nodes are given as the roots of $P_{N+1}(x)$. Consequently, the $(N-1)$ nodes are chosen as the roots of the polynomial $P'_N(x)$. Gauss-Lobatto is chosen because it requires less function evaluations than standard Gauss quadrature. Given two integers *M* and *L*, a Padè-Legendre approximation of a function u is the ratio of two approximating polynomials $\mathcal{P}_M$ and $\mathcal{Q}_L$ based on the Legendre basis. The overall order of the reconstruction is $N = (M + L + 1)$. Once the polynomial representation of the underlying function is obtained, it is possible to obtain mean $\tilde{u}$ and variance $\tilde{\sigma}$ directly from the function u:

$$\tilde{u} = \int_D u(x,\omega) f_\omega d\omega \quad and \quad \tilde{\sigma} = \int_D u(x,\omega)^2 f_\omega d\omega - \left[\int_D u(x,\omega) f_\omega d\omega\right]^2 \tag{8}$$

In Eq. 8, ω is the random parameter associated to the Probability Density Function f_ω, D represents the domain of the random parameters and x is the physical space.

UNCERTAINTY QUANTIFICATION RESULTS

The aim of this section is to evaluate how manufacturing deviations affect the film cooling effectiveness distribution of a cooling device. The uncertainty quantification analysis has been performed by considering both the diameters of the TE and the diameter of the coolant channel as independent random variables. Both deviations are considered to obtain a uniform distribution. Film cooling effectiveness has been extracted on the centreline of the passage and compared with corresponding experimental data provided by Ochs *et al.* (2007) for the baseline configuration. The deviations related to the geometrical parameters has been assumed as 10% of the nominal value for the coolant diameter and 20% for the trailing edge diameter. The test matrix of the simulated cases is summarized in Table 1, where also the BR values obtained by CFD are reported. As a first result of the UQ activity, it can be observed that blowing ratio seems to be independent from the deviation of the trailing edge dimension, but is considerably affected by the diameter of the coolant.

Table 1: Test matrix configuration, TE and coolant diameter

	$D_{TE,ND}$ [-]	$D_{C,ND}$ [-]	BR_{CFD} [-]
Grid 1	1.2	0.9	0.97
Grid 2	1.2	1.0	0.77
Grid 3	1.2	1.1	0.68
Grid 4	1.0	0.9	1.04
(Baseline) Grid 5	1.0	1.0	0.83
Grid 6	1.0	1.1	0.69
Grid 7	0.8	0.9	1.01
Grid 8	0.8	1.0	0.82
Grid 9	0.8	1.1	0.70

The presence of the shock induces a nonlinear behaviour of the deviation of film cooling effectiveness with respect to the deviation of geometrical parameters. Figure 5 shows the centreline adiabatic effectiveness predicted considering all the simulations. As previously reported, the shock position is determined in correspondence of a non-negligible variation of the centreline film cooling adiabatic effectiveness. Numerical data suggest that the shock impingement position is located approximately at x/D = 5.0 for all the investigated cases, while the experiments would suggest x/D = 8.0. It can be also observed that a small (but not negligible) variation in the slope appears x/D = 8.0 for the simulations (mainly Grid 2 and Grid 8, that differ by the TE diameter), while experiments show a limited slope change at x/D = 5.0. Furthermore, looking at Figure 1b and Figure 3b, it is clearly visible that, in the impingement region, the shock tends to change from oblique to normal, with increased intensity and impact on boundary layer thickness. It can be concluded that experimental and numerical data show that the shock effect is not confined to a certain position, but modifies the cooling performance in a region between x/D = 5.0 and x/D = 8.0. Furthermore, numerical data are affected by geometrical uncertainties, then a direct comparison between deterministic CFD and experimental data could provide incorrect information about local interaction. For these reasons, UQ methodologies have been used to reconstruct the centreline adiabatic effectiveness distribution based on the available CFD data.

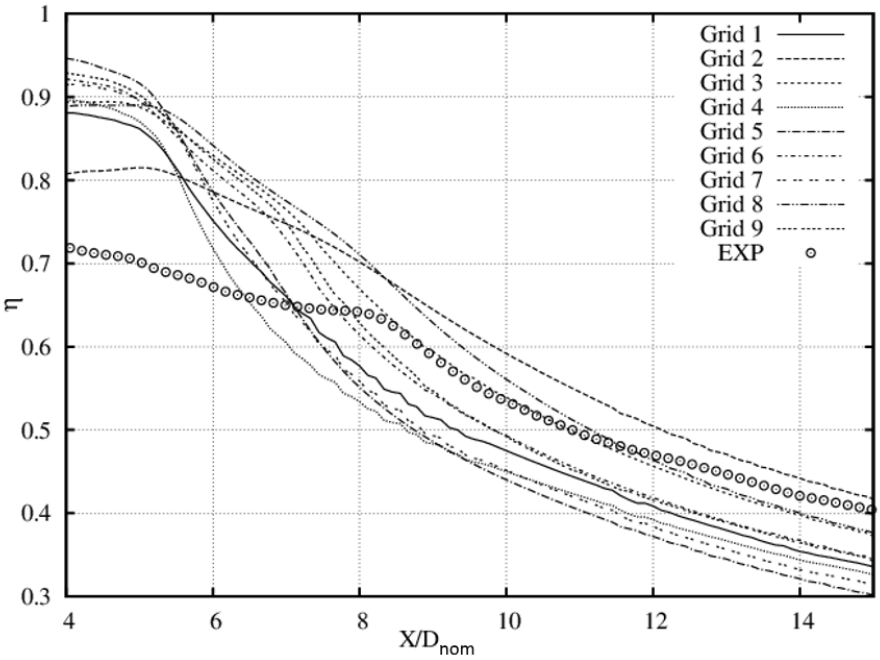

Figure 5: Centerline adiabatic film cooling effectiveness for the analysed cases

Figure 6 and Figure 7 show the statistical analysis of the effect of the diameter of the coolant and of the diameter of the trailing edge, respectively. The reconstructed distribution and the second moment of the distribution are shown. Comparing the standard deviations of Figure 6 and Figure 7, the stronger effect is related to the diameter of the hole. More consideration can be done by dividing the domain in three regions: upstream of the shock region, the shock region itself and downstream of the shock region. Looking at the standard deviation distributions it can be observed that the shock impingement region is confined between x/D = 5.0 and x/D = 8.0, coherently with the comments above. Furthermore, the distribution of the film cooling effectiveness in the location upstream of the shock is characterized by a high σ value for the case where the coolant diameter is changing (Figure 7). Lower values of σ characterize the case with TE deviation (Figure 6). A possible explanation for that behaviour is that upstream of the shock, the main effect is due to the jet penetration that is strongly perturbed by the variation of the coolant diameter, which affects also the shock position (for the blockage induced by the coolant) and consequently the film cooling

effectiveness. The impact of the trailing edge diameter could be underestimated by the fact that calculations are steady, and then the impact of modification of the plate vortex shedding is neglected.

The slope changes that are visible for both the reconstructed distribution (and delimit the shock region) have a double impact in terms of standard deviations. In correspondence of the shock the cooling flow is suddenly pushed towards the wall and this corresponds to the minimum value of σ. The subsequent adverse pressure gradient creates the already described lift-off mechanism, which is characterized by the presence of high vorticity. These vortices alter the surface coverage and the adiabatic effectiveness, and consequently the distribution has high value of σ. The shock region is greatly affected by the uncertainty due to the variation of the shock location, which deviates more for the case in Figure 6 because of the variation of the channel dimension.

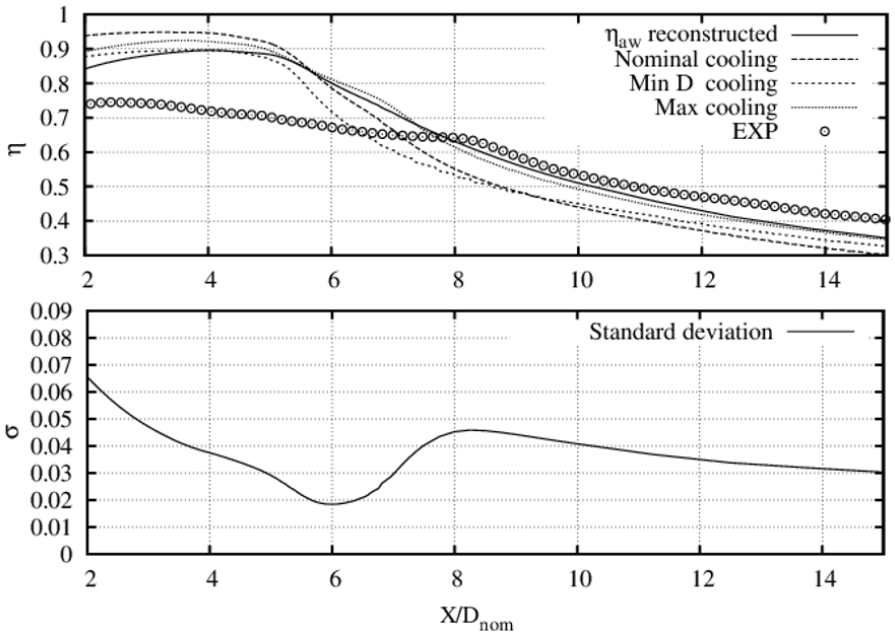

Figure 6: Statistics related to the influence of the diameter of the cooling hole

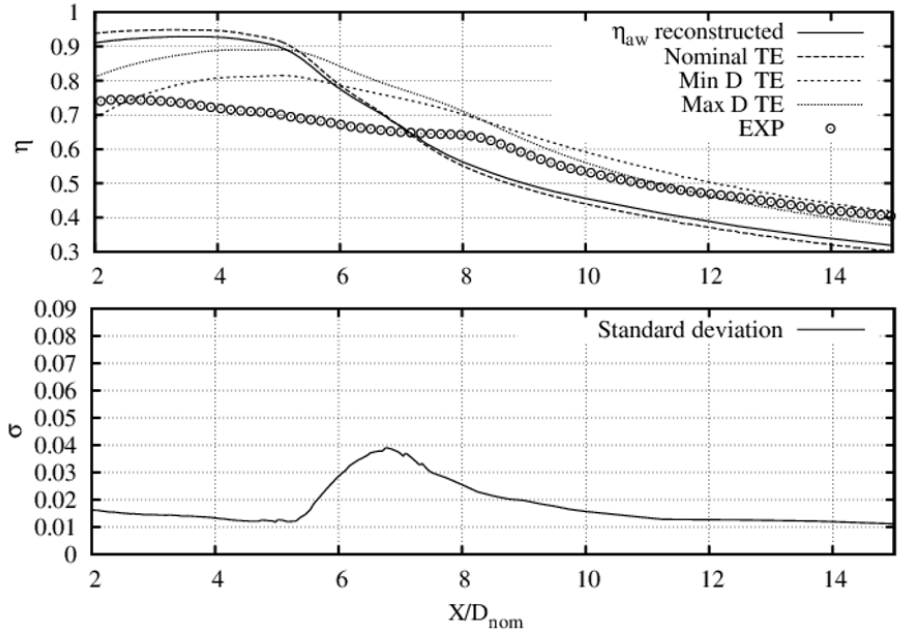

Figure 7: Statistics related to the influence of the deviation of TE diameter

CONCLUSIONS

This work provides a detailed insight of a film cooling jet interacting with a shock that impinges on a contoured plate. Results obtained by CFD highlight complex structures due to vorticity development inside of the coolant channel and to the subsequent interaction with the shock in the supersonic region. Deterministic calculations show that the coolant flow is detached from the end-wall in correspondence of the shock impingement. Kidney vortices are responsible for the reduction of cooling efficacy starting from the region upstream of the shock, then the local interaction with the shock and the generation of tornado-like vortices causes a further deterioration of film cooling performance. The flow structures occurring in the shock region are expected to be strongly dependent on geometrical parameters. The impact of manufacturing deviations altering the size of the hole and the trailing edge diameter is accounted for. Deterministic calculations performed by varying those parameters show that the impact of the shock is not limited to a certain location, but is responsible for a double slope change of centreline effectiveness in a region large about three nominal hole diameters. That result is supported also by the available experimental data. Looking at the deterministic data, it can be concluded that steady RANS calculation can individuate the region of influence of the shock, although this is obtained without the correct evaluation of shock intensity due to missing nonlinear, unsteady stress terms.

The complete numerical campaign consists in nine calculations and has been used to perform uncertainty quantification of cooling efficacy. The selected statistical approach is suitable for investigation of shock dominated flows. The results show different level of uncertainty in different zones of the domain. The zone upstream the shock is insensitive to the deviation of the trailing edge but it is strongly affected by the cooling flow penetration which is strictly related to cooling diameter. The shock generates an increase in the boundary layer height, which evolves in a lift mechanism that increases the uncertainty in the evaluation of adiabatic effectiveness. Furthermore, the deviation of the diameter of the coolant has a greater effect on the uncertainty of the shock location and strength with respect to the deviation of the dimension of the trailing edge of the shaped plate. As a general conclusion, the proposed uncertainty quantification methodology demonstrated to be a useful tool to understand the flow phenomena occurring in presence of film cooling devices and impinging shocks.

ACKNOWLEDGMENTS

The authors acknowledge the European Commission and the TATEF2 project consortium for support provided. The authors are also grateful to Prof. Francesco Martelli from the Department of Industrial Engineering of the University of Florence for his valuable contribution.

REFERENCES

Abramowitz, M., Stegun, I.A., 1964. *Handbook of Mathematical Functions with Formulas, Graphs, and Mathematical Tables*. Chapter **25.4**: *Integration*, Dover Publications, Inc., New York, ISBN 0-486-61272-4

Acharya, S., Leedom, D.H., 2012. *Large Eddy Simulations of Discrete Hole Film Cooling with Plenum Inflow Orientation Effects*. J. Heat Transfer **135(1)**, 011010 (12 pages) [DOI:10.1115/1.4007667]

Andreopulos, J., Rodi, W., 1984. *Experimental Investigation of Jets in a Crossflow*. J. Fluid Mechanics **138**, pp. 93-127 [DOI:10.1017/S0022112084000057]

Carnevale, M., Montomoli, F., D'Ammaro, A., Salvadori, S., Martelli, F., 2013. *Uncertainty Quantification: A Stochastic Method for Heat Transfer Prediction using LES*. ASME J. Turbomachinery **135(5)**, 051021 (8 pages) [DOI:10.1115/1.4007836]

Carnevale, M., D'Ammaro, A., Montomoli, F., Salvadori, S., 2014. *Film Cooling and Shock Interaction: An Uncertainty Quantification Analysis with Transonic Flows*. Proc. of the ASME

Turbo Expo 2014, Dusseldorf, Germany, June 16-20, Volume **5B**: Heat Transfer, V05BT13A001 (8 pages) [DOI:10.1115/GT2014-25024]

Chantrasmi, T., Doostan, A., Iaccarino, G., 2009. *Padè-Legendre Approximants for Uncertainty Analysis with Discontinuous Response Surface*. J. Computational Physics **228**, pp. 7159-7180 [DOI:10.1016/j.jcp.2009.06.024]

Chen, C.P., Blackwelder, R.F., 1978. *Large-Scale Motion in a Turbulent Boundary Layer: A Study using Temperature Contamination*. J. Fluid Mechanics **89(1)**, pp. 1-31 [DOI:10.1017/S0022112078002438]

Garg, V.K., Rigby, D.L., 1998. *Heat Transfer on a Film-Cooled Blade – Effect of Hole Physics*. International J. Heat Fluid Flow **20(1)**, pp. 10–25 [DOI:10.1016/S0142-727X(98)10048-6]

Hagen, J.P., Kurosaka, M., 1993. *Corewise Cross-Flow Transport in Hairpin Vortices – The "Tornado Effect"*. Physics of Fluids, **5(12)**: pp. 3167-3174 [DOI:10.1063/1.858673]

He, L., 2003. *Unsteady Flow and Aeroelasticity*. Chapter **5**, *Handbook of Turbomachinery*, CRC Press, ISBN 978-0-824-70995-2

Hesthaven, J.S., Kaber S.M., Lurati L., 2006. Padè-Legendre Interpolants for Gibbs reconstruction. J. Scientific Computing **28(2/3)**, pp. 337-359 [DOI:10.1007/s10915-006-9085-9]

Lamyaa, A.E.-G., Heidmann, J.D., 2013. *Numerical Study on the Sensitivity of Film Cooling CFD Results to Experimental and Numerical Uncertainties*. International J. Computational Methods Engineering Science Mechanics, **14(4)**, pp. 317-328 [DOI:10.1080/15502287.2012.756953]

Launder, B.E., Reece, G.J., Rodi, W., 1975. *Progress in the Development of a Reynolds-Stress Turbulence Closure*. J. Fluid Mechanics **68(3)**, pp. 537–566 [DOI:10.1017/S0022112075001814]

Leboeuf, F., Sgarzi, O., 2001. *The Detailed Structure and Behavior of Discrete Cooling Jets in a Turbine*. Annals New York Academy of Sciences **934**, pp-95-109

Ligrani, P.M., Saumweber, C., Schulz, A., Wittig, S., 2001. *Shock Wave–Film Cooling Interactions in Transonic Flows*. ASME J. Turbomachinery **123(4)**, pp. 788-797 [DOI:10.1115/1.1397305]

Montis, M., Ciorciari, R., Salvadori, S., Carnevale, M., Niehuis, R., 2014. Numerical Prediction of Cooling Losses in a High-Pressure Gas Turbine Airfoil. Proc. of IMechE, Part A: J. Power Energy **228(8)**, pp. 903–923 [DOI:10.1177/0957650914542630]

Montomoli, F., Massini, M., Salvadori, S., Martelli, F., 2012. *Geometrical Uncertainty and Film Cooling: Fillet Radii*. ASME J. Turbomachinery **134(1)**, 011019 (8 pages) [DOI:10.1115/1.4003287]

Montomoli, F., Carnevale, M., D'Ammaro, A., Massini, M., Salvadori, S., 2015. *Uncertainty Quantification in Computational Fluid Dynamics and Aircraft Engines*. Springer International Publishing, ISBN 978-3-319-14680-5

Ochs, M., Schulz, A., Bauer, H.-J., 2007. *Investigation of the Influence of Trailing Edge Shock Waves on Film Cooling Performance of Gas Turbine Airfoils.* Proc. of the ASME Turbo Expo 2007, Montreal, Canada, May 14–17, Volume **4**: Turbo Expo 2007, Parts A and B, pp. 465-474 [DOI:10.1115/GT2007-27482]

Salvadori, S., Montomoli, F., Martelli, F., Adami, P., Chana, K.S., Castillon, L., 2011. *Aerothermal Study of the Unsteady Flow Field in a Transonic Gas Turbine with Inlet Temperature Distortions*. ASME J. Turbomachinery **133(3)**, 031030 (13 pages) [DOI:10.1115/1.4002421]

Salvadori, S., Montomoli, F., Martelli, F., 2013. *Film Cooling Performance in Supersonic Flows: Effect of Shock Impingement*. Proc. of IMechE, Part A: J. Power Energy **227(3)**, pp. 295-305 [DOI:10.1177/0957650912474444]

Wilcox, D.C., 1994. *Simulation of Transition with a Two-Equation Turbulence Model*. AIAA Journal **32(2)**, pp. 247-255 [DOI:10.2514/3.59994]